Two- and Three-Dimensional Simulations of Vortex-Induced Vibration of a Circular Cylinder

H.M. BLACKBURN

Department of Mechanical Engineering, Monash University,
Melbourne, Australia

G.E. KARNIADAKIS

Department of Mechanical and Aerospace Engineering, Princeton University,
Princeton, New Jersey, USA

Abstract

Numerical simulations of the interaction between a circular cylinder and its wake during both forced and free, vortex-induced, oscillation have been performed using a spectral element method in which the computational mesh was fixed to the cylinder and the Navier-Stokes equations solved in this accelerating reference frame. Thus far, work has focussed on cross flow, rather than in-line oscillations; with forced oscillation the lock-in phenomenon was observed over a range of reduced velocities near critical, while for the freely-vibrating cylinder the amplitude-limiting phenomenon observed in experiments was reproduced. A comparison of free and forced oscillation has been performed in which the forced oscillation amplitude and frequency were set to match those achieved in free vibration; the forces exerted on the cylinder by the fluid were similar in each case. Initial simulations were two-dimensional but the method may also be applied to three-dimensional flows by employing a spectral element/Fourier representation.

Keywords: Circular cylinder lock-in spectral element vortex vibration.

1 Introduction

Vortex-induced vibration of slender circular-cylindrical structural elements is an important consideration in the design of many offshore structures, for both the fabrication/transport and operational phases. Despite the relatively fundamental nature of the problem, a comparatively small amount is known about the nature of the fluid-structure interaction, and the design rules which exist (e.g., CIRIA 1978) are based on a limited set of experimental results, such as those reviewed by King (1977). Partly as a result of the lack of understanding of the phenomenon, apparently unrelated sets of design procedures are available for structures immersed in flows of water (e.g., CIRIA) and air (e.g., ESDU 1985).

Various experimental techniques have been employed in past approaches to the problem of prediction of response amplitudes in vortex-induced vibration, employing both free-vibration testing (Feng 1968, King 1977) and experiments in which forced oscillations (exclusively in either cross flow or streamwise directions) were imposed (Bishop & Hassan 1964, Sarpkaya 1978, Blackburn 1992). The connection between the two has not been easy to establish, but attempts have been made to predict free-vibration amplitudes on the basis of measurements of forces obtained in forced oscillation tests (e.g., Staubli 1983). The outcome of these attempts has been uncertain, since, as noted by Bearman (1984), in no case has the same experimental setup been used for both the forced oscillation and free-vibration tests. This rather surprising fact is in part a result of the difficulty in designing an experimental rig satisfactory for both tasks. The measurement of fluid forces acting on a freely-vibrating cylinder is also difficult to arrange, and to our knowledge has only been attempted once (Reid & Hinwood 1987).

Vortex shedding in flows past circular cylinders exhibits a great deal of similarity over a very wide range of Reynolds numbers, despite the variety of Reynolds transitions which affect it. Likewise the basic pattern of fluid-structure interaction seems to be similar over the observed range of Reynolds numbers, judging by the fact that the phenomena of frequency-sensitive wake switching in flows with forced cylinder oscillation (Ongoren & Rockwell 1988) and self-excited vibrations near the critical reduced velocity with amplitude-limiting behaviour as zero mass-damping is approached (Griffin 1992) appear to be universal.
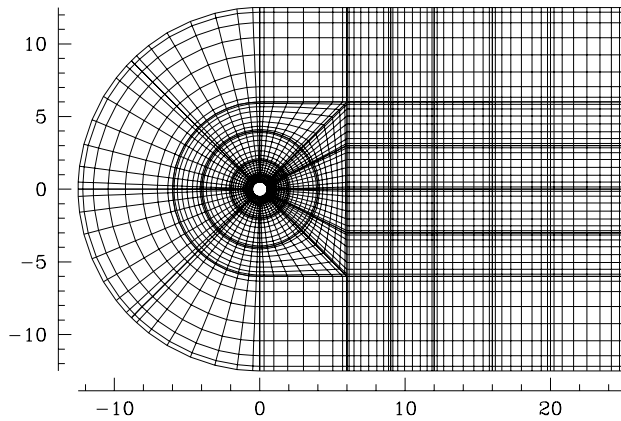
Given the difficulty with physical experiments

Figure 1: Computational mesh for domain Ω employed in the calculations, with dimensions conditions indicated. Layer of elements closest to cylinder have thickness $0.1\,D$.

and the apparent similarity of the phenomena over a range of Reynolds numbers, we have made a computationally-based approach to the problem, employing numerical simulations in which the cylinder could be forced to oscillate with given amplitudes and frequencies in the streamwise and cross flow directions or be left to execute free vibration in response to the forces exerted on it by the fluid. The main body of results reported here are for two-dimensional flow at $Re = 200$, but the extension to three-dimensional flow has been made, for which we report the numerical formulation. The method is equally applicable to the study of in-line or cross flow oscillations; in this paper we concentrate on the latter.

2   Problem Formulation

The computational domain Ω employed for the two-dimensional simulations is shown in Fig. 1; the domain extended a distance of $12.5\,D$ upstream and cross flow from the cylinder centreline, and a distance of $25\,D$ downstream. A large cross flow mesh dimension was employed to minimize blockage effects. Prescribed-velocity boundary conditions were used on the inflow, upper and lower boundaries while at the downstream end of the domain, outflow velocity and pressure boundary conditions were used, as indicated on the figure. For three-dimensional simulations the x-y planar projection of the mesh would be the same, with a number of planes spaced equally along the cylinder axis, in which direction the flow is assumed to be periodic.

Rather than arrange a method in which the computational grid deformed to allow cylinder motion, we have used a fixed-configuration grid attached to the cylinder. By applying appropriate boundary con-

ditions and adding a ficticious forcing term to the Navier-Stokes equations, the flow simulation may be carried out in this accelerating reference frame. The incompressible Navier-Stokes equations, written in rotational form for an inertial reference frame are

$$\frac{\partial \mathbf{u}}{\partial t} = -\nabla\Pi + \mathbf{u} \times \boldsymbol{\omega} + \nu\nabla^2\mathbf{u}, \qquad (1)$$

where $\Pi = p/\rho + \mathbf{u} \cdot \mathbf{u}/2$ and $\boldsymbol{\omega} = \nabla \times \mathbf{u}$. If the reference frame in which the Navier-Stokes equations are solved has a rectilinear acceleration $\mathbf{a}$, the equations become

$$\frac{\partial \mathbf{u}}{\partial t} = -\nabla\Pi + \mathbf{u} \times \boldsymbol{\omega} + \nu\nabla^2\mathbf{u} - \mathbf{a}. \qquad (2)$$

The appropriate velocity boundary conditions at prescribed-velocity boundaries are

$$\mathbf{u} = -\mathbf{v}, \qquad (3)$$

where $\mathbf{v}$ is the velocity of the reference frame. The pressure boundary condition is obtained by taking the normal component of (2), generated by dotting the unit normal boundary vector $\mathbf{n}$ into (2) to make

$$\frac{\partial \Pi}{\partial n} = \mathbf{n} \cdot [\mathbf{u} \times \boldsymbol{\omega} - \nu\nabla \times \boldsymbol{\omega}], \qquad (4)$$

where the form of the viscous term follows the suggestion of Orszag, Israeli and Deville (1986).

The force per unit length exerted by the pressure field on the cylinder is given by

$$\mathbf{f}_p = \oint p\mathbf{n}\,ds = \oint \rho\Pi\mathbf{n}\,ds, \qquad (5)$$

where $\mathbf{n}$ is again the unit outward normal of the fluid domain and the integration is performed around the circumference of the cylinder, while the viscous force per unit length is

$$\mathbf{f}_v = -\oint \mu\mathbf{n} \cdot [\nabla\mathbf{u} + (\nabla\mathbf{u})^T]\,ds. \qquad (6)$$

If the cylinder undergoes forced oscillation, the velocity and acceleration of the reference frame are given, however in the case of free vibration the mass, stiffness and damping of the cylinder must be considered and second order ODEs of the form

$$\ddot{\mathbf{x}} + 2\zeta\omega_n\dot{\mathbf{x}} + \omega_n^2\mathbf{x} = \mathbf{f}/m \qquad (7)$$

must be solved for each axis of motion, where for two-dimensional calculations m is the cylinder mass per unit length and $\mathbf{f} = \mathbf{f}_p + \mathbf{f}_v$ is the total force per unit length exerted by the fluid. Following normal practice these are decomposed into a set of first order ODEs with $\mathbf{v} = \dot{\mathbf{x}}$, giving

$$\begin{aligned} \dot{\mathbf{v}} &= \mathbf{f}/m - 2\zeta\omega_n\mathbf{v} - \omega_n^2\mathbf{x}, \\ \dot{\mathbf{x}} &= \mathbf{v}. \end{aligned} \qquad (8)$$

Here $\mathbf{v}$ is identical with the reference frame velocity since it is fixed to the cylinder.

The equations (2) are solved together with the incompressibility constraint

$$\nabla \cdot \mathbf{u} = 0 \quad \text{in} \quad \Omega. \tag{9}$$

This completes the problem formulation and describes the form used for the two-dimensional calculations. In the three-dimensional representation we have used, all variables are assumed to have periodicity in the z-direction (along the cylinder axis) and motion is constrained to the x and y directions. The cylinder is assumed prismatic, i.e., does not deform within its length. This approximates conditions near the centre-span of a slender elastic structural element in its first mode of free vibration. The dependent variables are represented in the three-dimensional formulation by

$$\left\{ \begin{array}{l} u(x,y,z,t) \\ v(x,y,z,t) \\ w(x,y,z,t) \\ p(x,y,z,t) \end{array} \right\} = \sum_{k=0}^{K-1} \left\{ \begin{array}{l} u(x,y,t) \\ v(x,y,t) \\ w(x,y,t) \\ p(x,y,t) \end{array} \right\} e^{i\beta k z} \tag{10}$$

where the spanwise wavenumber $\beta = 2\pi/L_z$. The Navier-Stokes equations (2) and the incompressibility constraint (9) then become sets of equations to be solved for each Fourier mode k;

$$\frac{\partial \mathbf{u}_k}{\partial t} = -\tilde{\nabla}\Pi_k + [\mathbf{u} \times \boldsymbol{\omega}]_k +$$
$$\nu \left[\nabla_{xy}^2 - k^2\beta^2 \right] \mathbf{u}_k - \mathbf{a}_k \quad \text{in} \quad \Omega_k, \tag{11}$$

$$\tilde{\nabla} \cdot \mathbf{u}_k = 0 \quad \text{in} \quad \Omega_k, \tag{12}$$

where the operators $\tilde{\nabla}$ and ∇_{xy}^2 are defined as

$$\tilde{\nabla} = \left(\frac{\partial}{\partial x}, \frac{\partial}{\partial y}, ik\beta \right), \quad \nabla_{xy}^2 = \frac{\partial^2}{\partial x^2} + \frac{\partial^2}{\partial y^2}. \tag{13}$$

The computational domain Ω_k is a projection onto the x-y plane of Ω, hence is the same for each mode. Since the reference frame acceleration $\mathbf{a}$ has components only in the x-y plane, $\mathbf{a}_k = 0$, $k \neq 0$.

Communication of information between modes is required only during the formulation of the $[\mathbf{u} \times \boldsymbol{\omega}]_k$ terms, when the products are formed in physical space, so that computations for each mode may be run in parallel except for the communication required during this step. The calculations performed for each mode are very similar to those for a two-dimensional calculation.

In three dimensions the integrals in (5) and (6) are extended to include the spanwise dimension; m becomes the total mass of the cylinder and $\mathbf{f}$ becomes the total force exerted by the fluid on the cylinder, but due to the use of Fourier expansions in the z direction, the form of the computation is exactly the same as in two dimensions, since the integrals need to be evaluated only for the $k = 0$ mode.

2.1 Discretization

A three-level high-order time-split scheme with a stiffly-stable semi-implicit integration method, described by Karniadakis, Israeli and Orzsag (1991), was employed for time integration of the Navier-Stokes equations. We give the three-dimensional Fourier-mode formulation; restriction to two dimensions is straightforward. The first sub-step deals with the nonlinear terms and the frame acceleration

$$\frac{\hat{\mathbf{u}}_k - \sum_{q=0}^{J-1} \alpha_q \mathbf{u}_k^{n-q}}{\Delta t} = \sum_{q=0}^{J-1} \beta_q \left[\mathbf{u} \times \boldsymbol{\omega} - \mathbf{a} \right]_k^{n-q}; \tag{14}$$

α_q and β_q are implicit/explicit weights for a stiffly-stable scheme of order J. The next substep recognizes the influence of the gradient of total pressure and the incompressibility constraint:

$$\begin{aligned} \frac{\hat{\hat{\mathbf{u}}}_k - \hat{\mathbf{u}}_k}{\Delta t} &= -\tilde{\nabla}\Pi_k^{n+1} \\ \tilde{\nabla} \cdot \hat{\hat{\mathbf{u}}}_k &= 0. \end{aligned} \tag{15}$$

The incompressibility constraint is applied to the first of this set of equations to produce a Helmholtz equation which must be solved for the total pressure, subject to the mode-equivalent of (4). The last sub-step incorporates the viscous correction and velocity boundary conditions;

$$\frac{\gamma_0 \mathbf{u}_k^{n+1} - \hat{\hat{\mathbf{u}}}_k}{\Delta t} = \nu \left[\nabla_{xy}^2 - k^2\beta^2 \right] \mathbf{u}^{n+1} \tag{16}$$

with boundary velocities $-\mathbf{v}$, $k = 0$ and identically zero for the higher modes. Here γ_0 is a weight in the backward differentiation employed in the stiffly-stable scheme.

The stiffly-stable scheme was also used for integration of the body-motion ODEs (8), with explicit extrapolation used to approximate displacements, lift and drag forces at the new time level;

$$\frac{\gamma_0 \mathbf{v}^{n+1} - \sum_{q=0}^{J-1} \alpha_q \mathbf{v}^{n-q}}{\Delta t} = -2\zeta\omega_n \mathbf{v}^{n+1} -$$
$$\sum_{q=0}^{J-1} \beta_q \left[\omega_n^2 \mathbf{x}^{n-q} - \frac{\mathbf{f}^{n-q}}{m} \right] \tag{17}$$

$$\frac{\gamma_0 \mathbf{x}^{n+1} - \sum_{q=0}^{J-1} \alpha_q \mathbf{x}^{n-q}}{\Delta t} = \mathbf{v}^{n+1}. \tag{18}$$

Minimal additional computation was required for the ODEs. In most cases second-order integration ($J = 2$) was used with dimensionless time steps $\Delta t U/D = 0.005$. At high amplitudes of forced oscillation ($\sim 0.5\,D$) and for free-vibration with low values of the density ratio $m/\rho D^2$ it was sometimes necessary to use first-order integration with time steps of 0.002 in order to maintain stability. Tests showed that the results were well-resolved in time. Since for

all Fourier modes other than the zeroth the integrations in (5) and (6) are zero when extended to three dimensions, the calculations needed for integration of the ODEs (8) may be restricted to the processor which carries the zeroth Fourier mode in a parallel computation.

A spectral element scheme (Karniadakis 1990, Henderson 1993), formed the basis for discretization in the x and y directions. 86 macro-elements were used, as shown in Fig. 1; eighth-order Legendre-Lagrangian polynomial tensor-product interpolants were used within each element (81 collocation points per element). In trials with tenth-order interpolants (121 points per element) agreement to within 1% in Strouhal number, lift and drag forces was obtained in two-dimensional computations with a stationary cylinder; hence it was decided that the eighth-order interpolant gave sufficient spatial resolution.

3 Forced Oscillation Results

The results in this and the two following sections relate to the two-dimensional simulations at $Re = 200$. The Strouhal number $St = f_v U/D$ was 0.200, where f_v is the vortex shedding frequency.

A series of tests were carried out in which the cylinder was forced to oscillate cross flow at a range of reduced frequencies $f_r = f_m U/D$ near "critical", defined as that reduced frequency at which the forced oscillation or mechanical frequency f_m matches f_v. Three oscillation amplitudes were chosen: $0.1\,D$, $0.2\,D$, and $0.5\,D$ (the peak-to-peak amplitudes are twice these values). Five frequencies were used at the amplitudes $0.1\,D$ and $0.5\,D$, while 13 were employed to obtain a more detailed survey at amplitude $0.2\,D$, as shown in Fig. 2, where approximate frequency limits for which lock-in (frequency coalescence) occurred are illustrated also.

The forced oscillation had a substantial effect on lift and drag forces within the lock-in regime, as may be seen in Fig. 3 (a) where mean and standard deviation coefficients of drag $(C_d,\ C_d')$ and standard deviation coefficients of lift (C_l') are presented as functions of the frequency ratio f_m/f_v for an $0.2\,D$ amplitude of oscillation. Values found for the fixed cylinder are presented for comparison. Long-term motion-correlated lift forces were computed using least-squares techniques (Blackburn 1992) and from these the phase angle with which motion-correlated forces led cylinder velocity was computed as shown in Fig. 3 (b). The phase angle calculations show that a change of sign of power transfer from the fluid to the cylinder occurred at the critical frequency, as previously demonstrated in physical experiments. This phenomenon is associated with the rapid change in phase with respect to cylinder motion of vortex shedding observed near the critical frequency (Zdravkovich 1982, Ongoren & Rockwell 1988).
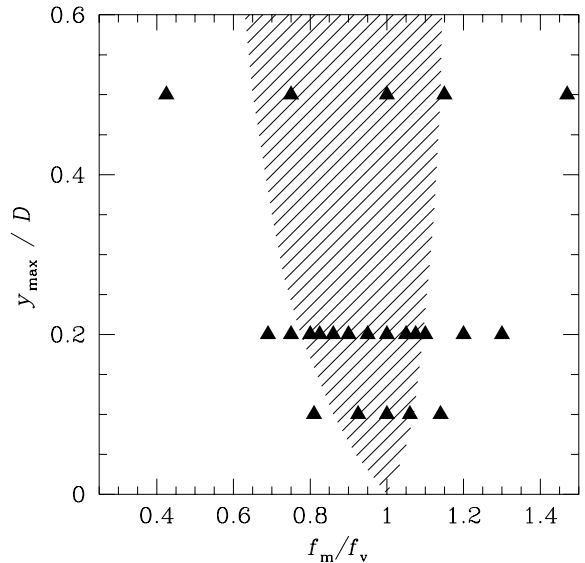

Figure 2: Frequency-amplitude envelope employed for forced-oscillation computations. Approximate limits within which lock-in was observed are shown shaded.
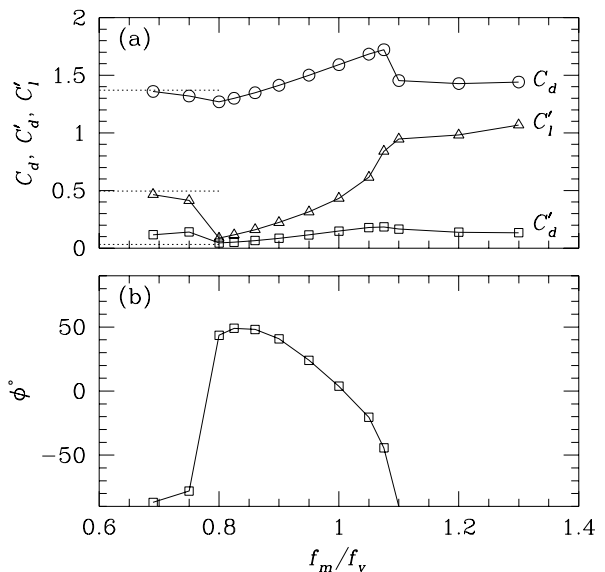

Figure 3: Results for forced oscillation at amplitude $0.2\,D$. (a); Mean and standard deviation coefficients of drag, C_d, C_d' and standard deviation of coefficient of lift, C_l', as functions of frequency ratio f_m/f_v. Fixed-cylinder values shown dashed for comparison. (b); Phase angle with which motion-correlated forces led cylinder velocity.
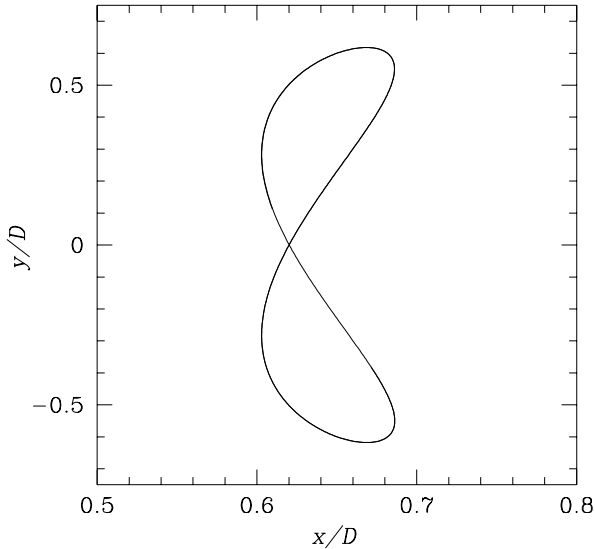
Figure 4: Free vibration cylinder centreline displacement phase portrait for $\zeta = 0.01$, $m/\rho D^2 = 1$.

4 Free Vibration

In the free vibration tests, the cylinder was released from rest in an established (steady amplitude, time-varying) flow field. The natural frequency of the cylinder, ω_n, was selected to match the vortex shedding frequency for the fixed cylinder. After release, cylinder oscillations grew in amplitude, with the time taken to reach steady state oscillation and maximum amplitudes being functions of the density ratio $m/\rho D^2$ and damping ratio ζ; transient times and maximum amplitudes increased with decreasing $m/\rho D^2$ and ζ. Steady state displacement, velocity and acceleration phase portraits had the general form of Lissajous figures generated by pairs of harmonic signals, one (streamwise direction) twice the frequency of the other, as illustrated for example in Fig. 4. Note the mean streamwise displacement, which is correct for the mean drag force and cylinder spring rate.

It is a well-established experimental result that steady-state amplitudes of cross flow and streamwise oscillation in free vibration increase toward maximum values in the limit $\zeta \rightarrow 0$. This is in contrast to what would be expected if there was no influence of cylinder motion on lift and drag forces, in which case it would be expected that amplitudes of oscillation would increase without bounds as damping reduced. To see if the computations would reproduce this behaviour, damping was reduced to low values, starting above the critical damping ratio, for two fixed values of density ratio, $m/\rho D^2 = 1$ and 10. The maximum steady-state peak-to-peak amplitudes are
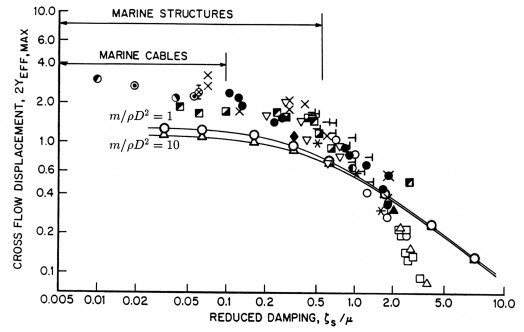

Figure 5: Maximum values of steady-state peak-to-peak free vibration oscillation amplitudes as functions of the mass-damping product $\zeta_s/\mu = 8\pi^2 St^2 m\zeta/\rho D^2$. A comparison of computed values for density ratios $m/\rho D^2 = 1$ and 10 with a compilation of experimental values reproduced from Griffin (1992).

shown as functions of the mass-damping product in Fig. 5, superimposed on a range of experimental results compiled by Griffin (1992). The nomenclature in his figure is slightly different to that which we have used; $\mathsf{Y}_{\text{EFF,MAX}}$ corresponds to $y_{\max}/D$ in the present paper, while ζ_s/μ corresponds to $8\pi^2 St^2 m\zeta/\rho D^2$.

The first point of note is that the general trend of the experimental values, namely the amplitude-limiting effect as $\zeta \rightarrow 0$, was reproduced by the computations, and that there is reasonable agreement between experimental and computed maximum amplitudes, considering the variation in Reynolds number between computations ($Re = 200$) and experiments $300 < Re < 10^6$. At high values of mass-damping the computed values tended to fall above the experimental values; we suspect this is related to three-dimensional wake flows in the physical experiments when oscillation amplitudes were low, which would have acted to reduce spanwise correlation and hence overall lift on a finite length of cylinder and thereby the amplitude of oscillation. Obviously this behaviour cannot be reproduced by a two-dimensional calculation. Finally it will be noted that variation of density ratio $m/\rho D^2$ had an observable effect, particularly at low damping ratios; lower values of density ratio gave rise to increased oscillation amplitudes. The justification for coalescence of density and damping ratios into a single parameter (e.g., $8\pi^2 St^2 m\zeta/\rho D^2$) is based in part on the assumption of simple harmonic motion; at lower values of $m/\rho D^2$ significant higher frequency components could be inferred from examination of acceleration timeseries and the characterization of amplitude by the single combined parameter becomes less valid.

5 Comparison of Free and Forced Oscillation

As mentioned in the Introduction, a comparison of lift and drag forces experienced by a cylinder in free vibration and forced oscillation at the same motion amplitude has never been conducted experimentally, however the present computational method provides an ideal vehicle for such a comparison. To perform this test, one set of results was selected as a basis for comparison; in this run the cylinder was free to vibrate in each axis of motion and the density and damping ratios were $m/\rho D^2 = 10$ and $\zeta = 0.01$. Steady-state oscillation amplitudes were 0.00475 and 0.434 in the streamwise and cross flow directions respectively, and the reduced frequency of cross flow oscillation was 0.199. Three comparisons were performed; in the first, the cylinder was also free to vibrate, but motion was restricted to the cross flow direction only; in the second, the cylinder was driven cross flow only, at the same frequency and amplitude as achieved in the base runs; finally the cylinder was driven in both the streamwise and cross flow directions with amplitudes and frequencies which matched those in base runs, while phase angle between the streamwise and cross flow motion was adjusted to be the same as for the base runs ($-45°$). The first case corresponds to free vibration tests in many experiments (as, e.g., Feng 1968), while the second corresponds to tests in most forced-oscillation experiments (e.g., Sarpkaya 1978).

A comparison of lift and drag force timeseries is presented in Fig. 6, together with the timeseries of lift and drag for a stationary cylinder; the magnitudes of fluctuating lift in all the cases for which the cylinder was in motion were significantly reduced from those observed for the fixed cylinder. This accords with the amplitude-limiting effect, as seen in Fig. 5; if lift forces did not reduce as amplitude of motion increased, motion amplitude in free vibration would grow without limit as $\zeta \to 0$, as noted above. The magnitudes of lift and drag were similar for all the cases in which the cylinder was in motion, as might be expected considering the comparatively small magnitude of streamwise oscillation and the almost pure harmonic motion experienced on each axis of motion in free vibration for the base case.

6 Conclusions

From the range of results presented here, we conclude that the computational method described is able to reproduce many of the phenomena observed experimentally in tests on cylinders in oscillation, both free and forced, in cross flow. It is planned to carry out a number of three-dimensional simulations for Reynolds numbers at which the wake flow is three-
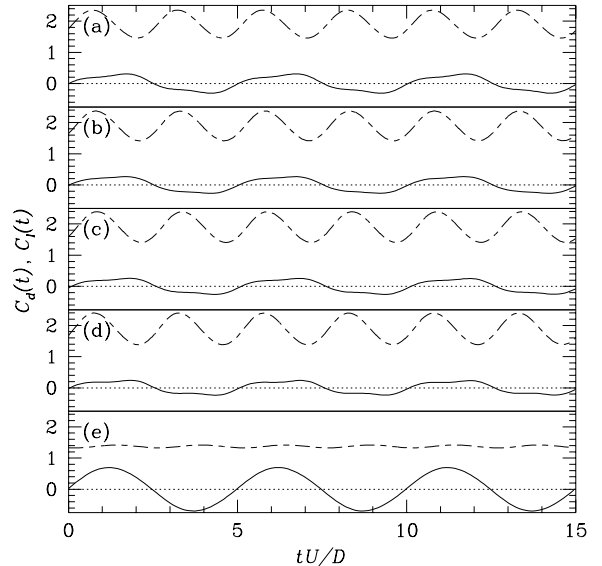

Figure 6: Timeseries of coefficients of lift and drag; the upper (dashed) line in each section is $C_d(t)$ and the lower is $C_l(t)$. (a); Base case, free vibration on both axes of motion with $m/\rho D^2 = 10$ and $\zeta = 0.01$, (b); Free vibration only on cross flow axis, (c); Forced oscillation in cross flow direction only, amplitude and frequency chosen to match base case, (d); Forced oscillation on both axes, with amplitudes, frequencies and phase angle chosen to match base case, (e); Results for fixed cylinder presented for comparison.

dimensional in order to assess the effect of cylinder motion on the flow, since it is known that the near wake tends to become more nearly two-dimensional when there is significant motion. Further work will extend the range of Reynolds number by introducing large eddy simulation, and extend the formulation to deal with oscillatory, rather than steady flow.

Besides observing the phenomena of coupling between cylinder motion and wake flows in both two and three dimensions it is planned to examine the physical mechanisms which account for the coupling and the suppression of three-dimensionality in the near wake region.

References

Bearman, P.W. 1984, Vortex shedding from oscillating bluff bodies, *Ann Rev Fluid Mech*, pp. 125–177.

Bishop, R.E.D. & Hassan, A.Y. 1964, The lift and drag forces on a circular cylinder oscillating in a flowing fluid, *Proc Roy Soc Lond A*, **277**, pp. 51–75.

Blackburn, H.M. 1992, Lift on an oscillating cylinder in smooth and turbulent flows, PhD thesis, Monash University.

Construction Industry Research and Information Association (CIRIA) 1978, *Report UR8 (2nd edn): Dynamics of Marine Structures.*

Engineering Sciences Data Unit (ESDU) 1985, *Item 85038: Circular-cylindrical structures: dynamic response to vortex shedding, Part 1.*

Feng, C.C. 1968, The measurement of vortex-induced effects in the flow past stationary and oscillating circular and D-section cylinders, MS thesis, University of British Columbia.

Griffin, O.M. 1992, Vortex-induced vibrations of marine structures in uniform and sheared currents, *NSF Workshop on Riser Dynamics*, University of Michigan.

Henderson, R.D. 1993, PhD thesis, Department of Mechanical and Aerospace Engineering, Princeton University.

Karniadakis, G.E. 1990, Spectral element-Fourier methods for incompressible turbulent flows, *Comp Methods in Appl Mech and Eng*, **80**, pp. 367–380.

Karniadakis, G.E., Israeli, M. & Orszag, S.A. 1991, High-order splitting methods for the incompressible Navier-Stokes equations, *J Comput Phys*, **97**, No 2, pp. 414–443.

King, R. 1977, A review of vortex-shedding research and its application, *Ocean Eng*, **4**, pp. 141–171.

Ongoren, A & Rockwell, D. 1988, Flow structures from an oscillating cylinder. Part 1. Mechanisms of phase shift and recovery in the near wake. *J Fluid Mech*, **191**, pp. 197–223.

Orzsag, S.A., Israeli, M. & Deville, M.O. 1986, Boundary conditions for incompressible flows, *J Sci Comput*, **1**, No 1, 75.

Reid, D.L. & Hinwood, J.B. 1987, An experimental rig for the study of fluid/structure interaction between elastic cylinders and ocean flows, in *Proc 8th A-Asian Conf Coastal & Ocean Eng*, Launceston, pp. 231–234.

Sarpkaya, T. 1978, Fluid forces on oscillating cylinders, *ASCE J Wat Port Coastal Ocean Div WW4*, **104**, pp. 275–290.

Staubli, T. 1983, Calculation of the vibration of an elastically mounted cylinder using data from forced oscillation, *ASME J Fluids Eng*, **105**, pp. 225–229.

Zdravkovich, M.M. 1982, Modification of vortex shedding in the synchronization range, *ASME J Fluids Eng*, **104**, pp. 513–517.